

# ACCURATE DETERMINATION OF HALO VELOCITY BIAS IN SIMULATIONS AND ITS COSMOLOGICAL IMPLICATIONS

JUNDE CHEN<sup>1,4,\*</sup>, PENGJIE ZHANG<sup>1,2,3,4,†</sup>, YI ZHENG<sup>5,6</sup>, YU YU<sup>1,4</sup>, YIPENG JING<sup>1,2,3,4</sup>

*Draft version July 4, 2018*

## ABSTRACT

A long-standing issue in peculiar velocity cosmology is whether the halo/galaxy velocity bias  $b_v = 1$  at large scale. The resolution of this important issue must resort to high precision cosmological simulations. However, this is hampered by another long-standing “sampling artifact” problem in volume weighted velocity measurement. We circumvent this problem with a hybrid approach. We first measure statistics free of sampling artifact, then link them to volume weighted statistics in theory, finally solve for the velocity bias.  $b_v$  determined by our method is not only free of sampling artifact, but also free of cosmic variance. We apply this method to a  $\Lambda$ CDM N-body simulation of  $3072^3$  particles and  $1200\text{Mpc}/h$  box size. For the first time, we determine the halo velocity bias to 0.1%-1% accuracy. Our major findings are as follows: (1)  $b_v \neq 1$  at  $k > 0.1h/\text{Mpc}$ . The deviation from unity ( $|b_v - 1|$ ) increases with  $k$ . Depending on halo mass and redshift, it may reach  $\mathcal{O}(0.01)$  at  $k = 0.2h/\text{Mpc}$  and  $\mathcal{O}(0.05)$  at  $k \sim 0.3h/\text{Mpc}$ . The discovered  $b_v \neq 1$  has statistically significant impact on structure growth rate measurement by spectroscopic redshift surveys, including DESI, Euclid and SKA. (2) Both the sign and the amplitude of  $b_v - 1$  depend on mass and redshift. These results disagree with the peak model prediction in that  $b_v$  has much weaker deviation from unity, varies with redshift, and can be bigger than unity. (3) Most of the mass and redshift dependences can be compressed into a single dependence on the halo density bias. Based on this finding, we provide an approximate two-parameter fitting formula.

*Keywords:* cosmology: observations: large-scale structure of universe: dark matter: dark energy

## 1. INTRODUCTION

A crucial (but often ignored) assumption in cosmology based on large scale peculiar velocity is that the galaxy/halo velocity bias  $b_v$  equals unity ( $b_v = 1$ ). The usual argument is based on the weak equivalence principle. On scales larger than about  $10\text{Mpc}$ , gravity is mainly dictated by the large scale distribution of dark matter in the Universe, instead of individual bound structures such as halos and galaxies. Therefore the motions of halos and galaxies should faithfully follow this large scale structure, leading to  $b_v = 1$  at  $\gtrsim 10\text{Mpc}$ .

Since galaxies/halos are not the dominant sources of gravity over  $\gtrsim 10\text{Mpc}$  scale, they can be treated as test particles. Therefore their motions should faithfully follow dark matter and therefore  $b_v = 1$  at  $\gtrsim 10\text{Mpc}$  scale.

However, this argument overlooks the fact that halos/galaxies only reside at (local) density peaks. Along with the fact that the density gradient is tightly correlated with the velocity field, the seminal BBKS (Bardeen et al. 1986) paper predicted  $\sigma_{v,\text{halo}}^2 < \sigma_{v,\text{matter}}^2$ . This result was derived using one-point Gaussian statis-

tics. Desjacques & Sheth (2010) (hereafter DS10) extended the peak model to 2-point statistics. They derived an elegant expression,  $b_v(k) = 1 - R_v^2 k^2 < 1$ . The prefactor  $R_v$  depends on the halo mass  $M$ , but not redshift. DS10 predicted significant and redshift independent deviation of  $b_v$  from unity, even at scales  $\gg 10\text{Mpc}$ . For example,  $b_v \simeq 0.93(0.73)$  at  $k = 0.1(0.2)h/\text{Mpc}$  for  $10^{13}M_\odot/h$  proto-halos (e.g. Elia et al. (2012)). Later theoretical and numerical works (Elia et al. 2012; Chan et al. 2012; Baldauf et al. 2014; Chan 2015) investigated and verified the DS10 prediction. Nonetheless, *these works are all for proto-halos defined in the linear and Gaussian initial conditions, instead of real halos which host galaxies in observations.* Due to stochastic relation between proto-halos and halos, and complexities in halo velocity evolution (e.g. Colberg et al. (2000)), ambiguities exist to extrapolate these works to peculiar velocities of real halos/galaxies.

Therefore, despite of decades of effort, the velocity bias remains an unresolved issue. Even worse, it will become a limiting factor of peculiar velocity cosmology in the near future (e.g. Howlett et al. (2017)). In particular, stage IV dark energy surveys such as DESI, PFS, Euclid, SKA and WFIRST (e.g. Schlegel et al. (2011); Spergel et al. (2015); Abdalla et al. (2015); DESI Collaboration et al. (2016); Amendola et al. (2016)) aim to measure the structure growth rate  $f(z)\sigma_8(z)$  to 1% or higher accuracy, through redshift space distortion (RSD). However, what RSD actually measures is the galaxy peculiar velocity and therefore the combination  $b_v \times f\sigma_8$ . Systematic bias in the understanding of  $b_v$  then induces a systematic

<sup>1</sup> Department of Astronomy, School of Physics and Astronomy, Shanghai Jiao Tong University, Shanghai, 200240

<sup>2</sup> IFSA Collaborative Innovation Center, Shanghai Jiao Tong University, Shanghai 200240, China

<sup>3</sup> Tsung-Dao Lee Institute, Shanghai 200240, China

<sup>4</sup> Shanghai Key Laboratory for Particle Physics and Cosmology

<sup>5</sup> School of Physics, Korea Institute for Advanced Study, Hoegiro 85, Seoul 02455, Korea

<sup>6</sup> Korea Astronomy and Space Science Institute, 776, Daedeokdae-ro, Yuseong-gu, Daejeon 34055, Republic of Korea

\* jundechen@sjtu.edu.cn

† zhangpj@sjtu.edu.cn

**Table 1**

Five sets of halo mass bins. The mass unit is  $10^{12} M_{\odot}/h$ .  $\langle M \rangle$  is the mean halo mass.  $N_h$  is the total number of halos in the corresponding mass bin.  $b_h$  is the halo density bias at  $k < 0.1h/\text{Mpc}$ .

| Set ID          | mass range | $\langle M \rangle$ | $N_h/10^9$ | $b_h(k < 0.1h/\text{Mpc})$ |
|-----------------|------------|---------------------|------------|----------------------------|
| A1( $z = 0.0$ ) | $> 10$     | 37.7                | 7.1        | 1.36                       |
| $z = 0.5$       | $> 10$     | 29.8                | 5.5        | 1.89                       |
| $z = 1.0$       | $> 10$     | 23.7                | 3.5        | 2.68                       |
| $z = 2.0$       | $> 10$     | 17.7                | 0.88       | 4.98                       |
| A2( $z = 0.0$ ) | 1-10       | 2.7                 | 54.4       | 0.81                       |
| $z = 0.5$       | 1-10       | 2.6                 | 52.5       | 1.04                       |
| $z = 1.0$       | 1-10       | 2.5                 | 46.9       | 1.48                       |
| $z = 2.0$       | 1-10       | 2.3                 | 28.6       | 2.64                       |
| A3( $z = 0.0$ ) | 0.5-1      | 0.70                | 52.9       | 0.70                       |
| $z = 0.5$       | 0.5-1      | 0.70                | 54.0       | 0.86                       |
| $z = 1.0$       | 0.5-1      | 0.69                | 52.4       | 1.15                       |
| $z = 2.0$       | 0.5-1      | 0.69                | 39.7       | 1.97                       |
| $z = 3.0$       | 0.5-1      | 0.68                | 21.8       | 3.15                       |
| B1( $z = 0.0$ ) | 0.5-1      | 0.70                | 52.9       | 0.70                       |
| B2( $z = 0.0$ ) | 1-7        | 2.4                 | 51.5       | 0.80                       |
| B3( $z = 0.0$ ) | 7-10       | 8.2                 | 3.3        | 1.02                       |
| B4( $z = 0.0$ ) | $> 10$     | 37.7                | 7.1        | 1.36                       |
| C1( $z = 0.0$ ) | 7-10       | 8.2                 | 3.3        | 1.02                       |
| C2( $z = 0.5$ ) | 1.2-4.0    | 2.1                 | 34.1       | 1.02                       |
| C3( $z = 1.0$ ) | 0.31-0.35  | 0.33                | 20.3       | 1.01                       |

error in  $f\sigma_8$ ,

$$\left. \frac{\delta(f\sigma_8)}{f\sigma_8} \right|_{k,z} \simeq - \left. \frac{\delta b_v}{b_v} \right|_{k,z}. \quad (1)$$

$b_v$  is in principle dependent of scale  $k$ . So the induced systematic error depends on the small scale cut  $k_{\text{max}}$  (namely we only use the velocity information at  $k \leq k_{\text{max}}$ ). Various cuts have been adopted in peculiar velocity cosmology. DESI Collaboration et al. (2016) adopts  $k_{\text{max}} = 0.2h/\text{Mpc}$  in DESI forecast. The eBOSS collaboration adopts  $0.3h/\text{Mpc}$  in the quasar power spectrum analysis, and  $r \sim 20\text{Mpc}/h$  in the quasar correlation function analysis (Gil-Marín et al. 2018; Ruggeri et al. 2018; Zhao et al. 2018; Hou et al. 2018; Zarrouk et al. 2018). Ambitious stage V dark energy projects (Dodelson et al. 2016) can measure RSD to smaller scales, and  $k_{\text{max}} = 0.5h/\text{Mpc}$  will further significantly improve cosmological constraints. To match the survey capability, we have to theoretically understand  $b_v$  at 0.1%-1% level accuracy over the range  $k \leq 0.2-0.5h/\text{Mpc}$ .

Since halos are highly nonlinear objects, we have to resort to high precision cosmological simulations to accurately measure their velocity statistics. State of art simulations are already able to reliably simulate the formation and evolution of halos hosting target galaxies in cosmological surveys, and generate accurate phase-space distribution of halos.

Nevertheless, translating the accurately simulated halo phase-space distribution into the volume weighted velocity statistics<sup>9</sup> is highly non-trivial, due to a long-

<sup>9</sup> Unlike the density weighted velocity statistics, the volume weighted velocity does not depend on the galaxy density bias. For theoretical modeling of RSD, the volume weighted velocity statistics is preferred in some approaches (e.g. Kaiser (1987); Scoccimarro (2004); Taruya et al. (2010); Zhang et al. (2013)), while the density weighted statistics is preferred in the distribution function approach (Seljak & McDonald 2011; Okumura et al. 2012) and the streaming model (Peebles 1980; White et al. 2015).

**Table 2**

The determined velocity bias. We discover statistically significant deviation of  $b_v$  from unity at  $k \geq 0.1h/\text{Mpc}$ .  $|b_v - 1|$  increases with  $k$ , and may reach  $\mathcal{O}(10\%)$  at  $k \sim 0.3h/\text{Mpc}$ .

| Set ID          | $(b_v - 1) \times 100$ | $(b_v - 1) \times 100$ | $(b_v - 1) \times 100$ |
|-----------------|------------------------|------------------------|------------------------|
|                 | $0.05 < k < 0.1$       | $0.15 < k < 0.2$       | $0.25 < k < 0.3$       |
| A1( $z = 0.0$ ) | $0.03 \pm 0.13$        | $-0.05 \pm 0.38$       | $-0.14 \pm 0.93$       |
| $z = 0.5$       | $-0.02 \pm 0.16$       | $-0.29 \pm 0.32$       | $-1.01 \pm 0.63$       |
| $z = 1.0$       | $-0.04 \pm 0.27$       | $-0.40 \pm 0.53$       | $-2.57 \pm 0.97$       |
| $z = 2.0$       | $-0.31 \pm 0.43$       | $-1.46 \pm 0.82$       | $-6.90 \pm 1.32$       |
| A2( $z = 0.0$ ) | $0.04 \pm 0.06$        | $0.37 \pm 0.12$        | $1.21 \pm 0.33$        |
| $z = 0.5$       | $0.07 \pm 0.06$        | $0.27 \pm 0.14$        | $0.81 \pm 0.19$        |
| $z = 1.0$       | $0.04 \pm 0.06$        | $0.06 \pm 0.08$        | $0.26 \pm 0.20$        |
| $z = 2.0$       | $-0.05 \pm 0.08$       | $-0.37 \pm 0.18$       | $-1.25 \pm 0.13$       |
| A3( $z = 0.0$ ) | $-0.01 \pm 0.06$       | $0.40 \pm 0.15$        | $1.50 \pm 0.19$        |
| $z = 0.5$       | $0.05 \pm 0.04$        | $0.35 \pm 0.13$        | $1.06 \pm 0.21$        |
| $z = 1.0$       | $0.04 \pm 0.05$        | $0.22 \pm 0.15$        | $0.60 \pm 0.17$        |
| $z = 2.0$       | $-0.04 \pm 0.07$       | $-0.08 \pm 0.15$       | $-0.31 \pm 0.15$       |
| $z = 3.0$       | $-0.12 \pm 0.10$       | $-0.60 \pm 0.22$       | $-1.58 \pm 0.26$       |
| B1( $z = 0.0$ ) | $-0.01 \pm 0.06$       | $0.40 \pm 0.15$        | $1.50 \pm 0.19$        |
| B2( $z = 0.0$ ) | $0.04 \pm 0.07$        | $0.33 \pm 0.14$        | $1.22 \pm 0.24$        |
| B3( $z = 0.0$ ) | $-0.01 \pm 0.28$       | $0.43 \pm 0.50$        | $0.57 \pm 1.03$        |
| B4( $z = 0.0$ ) | $0.03 \pm 0.13$        | $-0.05 \pm 0.38$       | $-0.14 \pm 0.93$       |
| C1( $z = 0.0$ ) | $-0.01 \pm 0.06$       | $0.43 \pm 0.50$        | $0.57 \pm 1.03$        |
| C2( $z = 0.5$ ) | $0.06 \pm 0.07$        | $0.34 \pm 0.17$        | $0.88 \pm 0.38$        |
| C3( $z = 1.0$ ) | $0.04 \pm 0.07$        | $0.29 \pm 0.22$        | $0.66 \pm 0.35$        |

standing problem of ‘‘sampling artifact’’. This problem exists for galaxies, halos and simulation particles. One way to demonstrate its existence is to randomly select a fraction  $f_{\text{sub}}$  of these objects and then measure the velocity power spectrum of this sub-sample. The measured velocity power spectrum should be independent of  $f_{\text{sub}}$ . However, both theoretical and numerical investigations show significant dependence, and therefore the existence of sampling artifact (Zhang et al. 2015; Zheng et al. 2015b). This sampling artifact problem arises from the fact that we only know the velocities where there are objects (halos, galaxies, simulation particles). Their distributions are not only inhomogeneous, but also correlated with their velocity fields. So the sampling of their velocity fields is biased, leading to biased measurement of volume weighted velocity statistics (e.g. Bernardeau & van de Weygaert (1996); Bernardeau et al. (1997); Schaap & van de Weygaert (2000); Pueblas & Scoccimarro (2009); Zheng et al. (2013); Zhang et al. (2015); Zheng et al. (2015b); Jennings et al. (2015)).

For the dark matter velocity statistics, this is essentially an issue of mass resolution. If on the average there are  $\gg 10$  simulation particles in a volume  $L^3$ , the velocity field above the scale  $L$  is well sampled and the sampling artifact is negligible. Increasing the mass resolution increases the number density of simulation particles and pushes the reliable measurement to smaller scales. Unfortunately, the sampling artifact in the halo velocity statistics is much worse and can not be reduced by increasing the mass resolution. First, halos are much more sparse than simulation particles, causing much severer sampling artifact. Second, increasing the mass resolution can not alleviate the sampling artifact problem, since the halo number density is fixed at given redshift and mass. This sampling artifact prohibits accurate determination of halo velocity bias in simulations, with existing methods.

We have tried various approaches to measure the vol-

ume weighted velocity statistics in simulations. We have designed new velocity assignment methods, including the NP method (Zheng et al. 2013) and the Kriging method (Yu et al. 2015, 2017). We have built theoretical model of the sampling artifact (Zhang et al. 2015), verified it in simulated dark matter velocity field (Zheng et al. 2015b) and then applied it to correct the sampling artifact in the halo velocity field (Zheng et al. 2015a). Despite these efforts, we have not yet succeeded in measuring  $b_v$  with 1% accuracy at  $k = 0.1h/\text{Mpc}$ . The  $b_v$  measurement at larger  $k$  is even more challenging.

The current paper presents an exact approach to determine  $b_v$  from simulations. It circumvents the problem of sampling artifact by a hybrid method. For the first time, we determine  $b_v(k, z)$  to 0.1%-1% at  $k \leq 0.4h/\text{Mpc}$  and  $0 < z < 2$ , for various halo mass bins. In §2, we present our method of determining  $b_v$ . We leave further technical details in the appendix. In §3 we describe the simulation used for the velocity bias measurement. In §4 we present the determined  $b_v(k)$  for various halo mass and redshift. In §5 we discuss its impact on cosmological surveys. We discuss and conclude in §6.

## 2. THE METHOD

The method is hybrid in the sense that it is composed of two steps, direct measurements and theoretical interpretation.

- Direct measurements are for three quantities, all with negligible sampling artifact. (1) One is the halo momentum  $\mathbf{p}_h \equiv (1 + \delta_h)\mathbf{v}_h$ . (2) One is the halo number overdensity  $\delta_h(\mathbf{x})$ , for which the sampling artifact is irrelevant. It is the density weighted velocity, free of sampling artifact. (3) One is the matter velocity  $\mathbf{v}_m$ . In principle it contains sampling artifact. Fortunately, it has been suppressed to a negligible level in our simulation. Our simulation has on the average 216 simulation particles per  $(2.4\text{Mpc}/h)^3$  volume. For such dense sampling, the resulting sampling artifact in the dark matter velocity power spectrum is  $0.02\% \times (k/(0.1h/\text{Mpc}))^2$  (estimated by Eq.16&24 in Zhang et al. (2015)). The induced systematic error in the determined  $b_v$  is half of that,  $0.01\% \times (k/(0.1h/\text{Mpc}))^2$ . Therefore the dark matter velocity field at scales of interest ( $k \lesssim 0.4h/\text{Mpc}$ ) is well sampled and is essentially free of sampling artifact.
- These direct measurements are then exactly linked to the volume weighted statistics in theory, where the only unknown parameter is  $b_v(k)$ . We then solve for  $b_v$ . The determination of  $b_v$  is then free of sampling artifact.

**Step 1.** We first measure the correlation function

$$\xi_{(1+\delta_h)v_h v_m}(r) \equiv \langle (1 + \delta_h(\mathbf{x}_1))\mathbf{v}_h(\mathbf{x}_1) \cdot \mathbf{v}_m(\mathbf{x}_2) \rangle \quad (2)$$

and its Fourier counterpart  $P_{(1+\delta_h)v_h v_m}(k)$ . These measurements are then linked to the following correlation functions

$$\xi_{(1+\delta_h)v_h v_m}(r) = \langle \mathbf{v}_h \cdot \mathbf{v}_m \rangle + \langle \delta_h \mathbf{v}_h \cdot \mathbf{v}_m \rangle \quad (3)$$

and their power spectra (Fourier components)

$$P_{(1+\delta_h)v_h v_m}(k) = P_{v_h v_m}(k) + B_{\delta_h v_h v_m}(k). \quad (4)$$

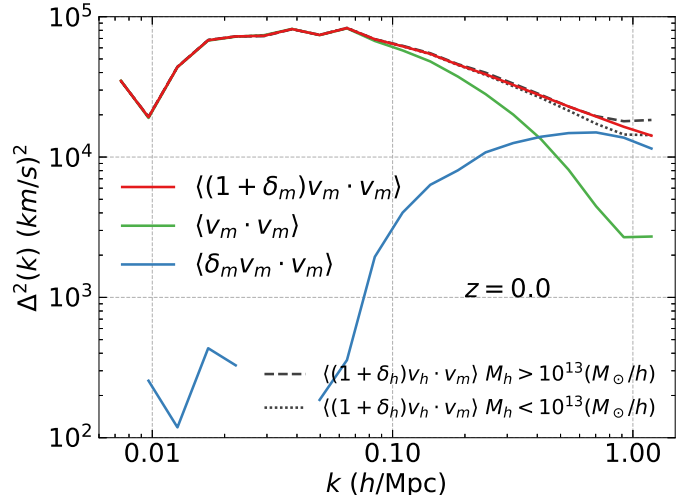


**Figure 1.** The  $z = 0$  power spectrum variance  $\Delta_\alpha^2 \equiv k^3 P_\alpha(k)/2\pi^2$  in unit of  $(\text{km/s})^2$ , where  $\alpha = (1 + \delta_m)v_m v_m$ ,  $(1 + \delta_h)v_h v_m$ ,  $v_m v_m$ ,  $\delta_m v_m v_m$ . All these measurements are essentially free of the sampling artifact in the velocity field. At  $k < 0.3h/\text{Mpc}$ ,  $P_{(1+\delta_m)v_m v_m}$  is dominated by  $P_{v_m v_m}$ . This property makes the measurement of  $b_v$  easier.

Here  $\langle \dots \rangle$  denote the volume/ensemble averaging.

**Step 2.** We then solve Eq. 4 for the velocity bias  $b_v(k)$ , defined through

$$b_v(k) \equiv \frac{P_{v_h v_m}(k)}{P_{v_m v_m}(k)}. \quad (5)$$

A key point to pay attention is that  $b_v(k)$  is the only unknown quantity in Eq. 4. The proof is presented in the appendix. Then comparing the left and right hand sides drawn from the same simulation, we determine  $b_v$ . For this reason, the determined  $b_v$  is essentially free of cosmic variance. In the appendix, we present the maximum likelihood approach to solve Eq. 4 for  $b_v(k)$ .

## 3. THE SIMULATION

The simulation we analyze (J6620) adopts the standard  $\Lambda\text{CDM}$  cosmology, with  $\Omega_m = 0.268$ ,  $\Omega_\Lambda = 0.732$ ,  $\Omega_b = 0.044$ ,  $\sigma_8 = 0.83$ ,  $n_s = 0.96$  and  $h = 0.71$ . It has box size  $L_{\text{box}} = 1200\text{Mpc}/h$ , particle number  $N_P = 3072^3$  and the mass resolution  $4.4 \times 10^9 M_\odot$ . J6620 is run with a particle-particle-particle-mesh (P<sup>3</sup>M) code, detailed in Jing et al. (2007). The halo catalogue is constructed by the Friends-of-Friends (FOF) method. The linking length is  $b = 0.2$ . In the catalogue gravitationally unbound ‘‘halos’’ have been excluded. The halo center is defined as the mass weighted center and the halo velocity is defined as the velocity averaged over all member particles. We adopt various mass and redshift bins to calculate the mass and redshift dependence of velocity bias. Table 1 shows details of these bins.

The number density and momentum fields of both halos and dark matter are measured using the NGP method. Namely  $(1 + \delta_h)\mathbf{v}_h = \sum_i \mathbf{v}_h^i / \bar{n}$ . The sum ( $\sum_i$ ) is over all particles in the given cell.  $\bar{n}$  is the mean number of halos in each cell. We adopt  $512^3$  grid points. The grid cell size is  $L_{\text{grid}} = 2.4\text{Mpc}/h$ . Each cell has 216 simulation particles on the average. Therefore we have excellent sampling of the dark matter velocity field above such scale. This allows us to

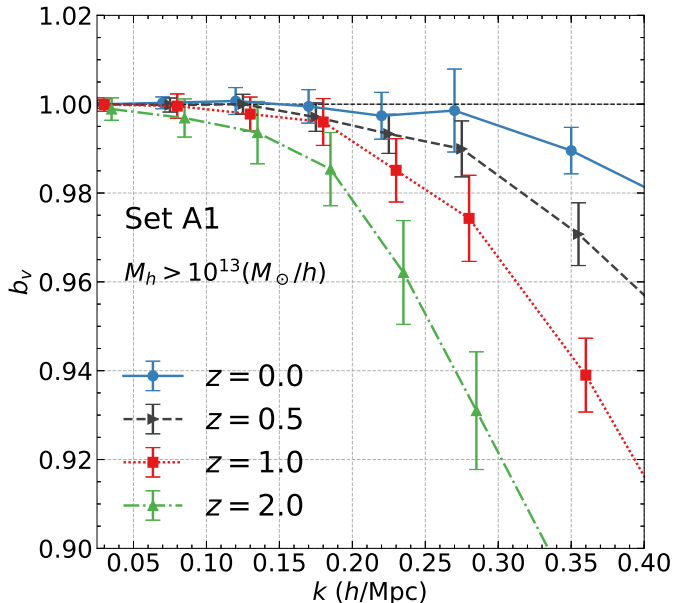


**Figure 2.** The velocity bias of halo set A1 ( $M > 10^{13} M_{\odot}/h$ ) at  $z = 0, 0.5, 1.0, 2.0$ . The velocity bias decreases with increasing redshift. For these halos,  $b_v < 1$  at all redshifts. Notice that for clarity we shift the  $z > 0$  data points horizontally. The result invalidates the usual assumption of  $b_v = 1$  in peculiar velocity cosmology.  $|b_v - 1|$  is much weaker than the peak model prediction. It also shows significant redshift evolution, in contrast to the peak model prediction.

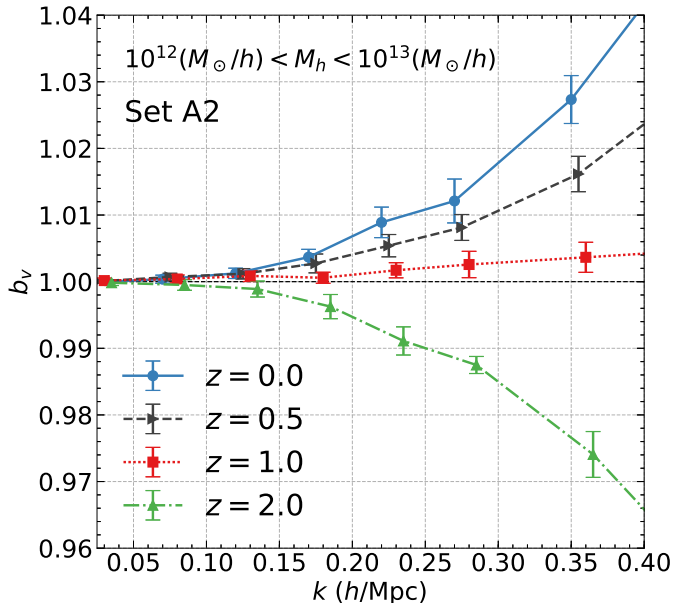


**Figure 3.** Similar to Fig. 2, but for halo set A2 ( $10^{12} < M/(M_{\odot}/h) < 10^{13}$ ). Notice that  $b_v - 1$  changes from positive sign to negative sign from  $z = 0$  to  $z = 2$ .

robustly measure the dark matter velocity field through  $\mathbf{v}_m = \sum_i \mathbf{v}_m^i / \sum_i$ , with negligible sampling artifact. The aliasing effect is also negligible, since we are interested in the scales of  $k \lesssim 0.4 h/\text{Mpc}$ , much smaller than the Nyquist wavenumber  $k_N = \pi/L_{\text{grid}} = 1.31 h/\text{Mpc}$  (Jing 2005).

Fig. 1 shows the directly measured  $P_{(1+\delta_h)v_h v_m}$  for  $M > 10^{13} M_{\odot}/h$  and  $10^{12} M_{\odot}/h < M < 10^{13} M_{\odot}/h$  halos

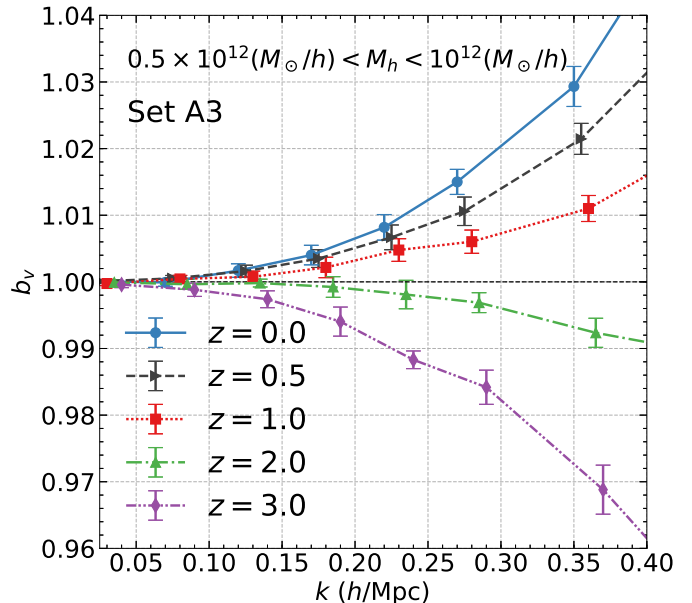


**Figure 4.** Similar to Fig. 2, but for set A3 ( $5 \times 10^{11} < M/(M_{\odot}/h) < 10^{12}$ ). Again,  $b_v - 1$  changes sign with redshift.

at  $z = 0$ . For comparison, we also show  $P_{(1+\delta_m)v_m v_m}$ . The three are almost identical to each other until  $k \gtrsim 0.2 h/\text{Mpc}$ . These terms have two contributions. The contribution from  $\langle \mathbf{v} \cdot \mathbf{v} \rangle$  dominates at  $k \lesssim 0.3 h/\text{Mpc}$ . The contribution from  $\langle \delta \mathbf{v} \cdot \mathbf{v} \rangle$  becomes significant at  $k \gtrsim 0.2 h/\text{Mpc}$  and becomes dominant at  $k \gtrsim 0.3 h/\text{Mpc}$ . These results already imply  $b_v \simeq 1$  at  $k \lesssim 0.1 h/\text{Mpc}$ . The exact determination of  $b_v(k)$  requires to solve Eq. 4 using the method described in the appendix.

#### 4. THE VELOCITY BIAS

We obtain the best-fit value and the associate error of  $b_v(k)$  over the  $k$  ranges of  $(0, 0.05)$ ,  $(0.05, 0.1)$ ,  $(0.1, 0.15)$ ,  $(0.15, 0.20)$ ,  $(0.20, 0.25)$ ,  $(0.25, 0.3)$ ,  $(0.3, 0.4)$ ,  $(0.4, \infty)$ . As explained early, the determined  $b_v$  is essentially free of cosmic variance, since it is obtained by comparing the halo and dark matter fields in the same simulation box. The only source of noise is shot noise in the halo distribution. The large number of halos ( $\sim 10^{5-7}$ ) then enables us to determine  $b_v(k \lesssim 0.4 h/\text{Mpc})$  with 0.1%-1% statistical error. Such accuracy also enables us to detect any significant deviation of  $b_v$  from unity.

Fig. 2, 3 & 4 show the redshift dependence of velocity bias for three mass bins (halo set A1, A2, A3 respectively). Fig. 5 shows the mass dependence of velocity bias at  $z = 0$  (set B). Furthermore, table 2 lists the velocity bias at selected ranges of  $k$ .

We detect statistically significant deviation of  $b_v$  from unity at  $k \geq 0.1 h/\text{Mpc}$ . This invalidates the assumption of  $b_v = 1$  commonly adopted in peculiar velocity cosmology. It will significantly impact RSD cosmology of stage IV dark energy projects. The deviation  $b_v - 1$  shows rich behavior in  $k$ , halo mass  $M$  and redshift  $z$ . Nonetheless, it shows significant difference to the peak model prediction and poses new question to the halo peculiar velocity theory. Major findings are as follows.

##### 4.1. The $k$ dependence

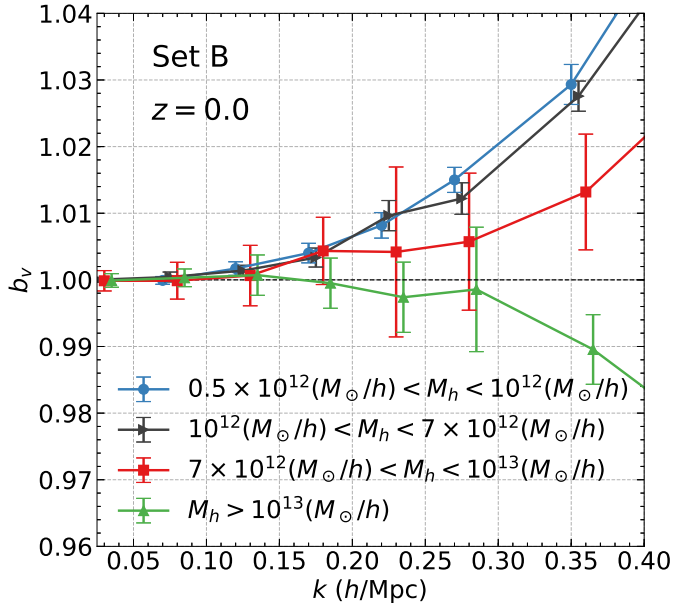


**Figure 5.** The dependence of halo velocity bias on halo mass (halo set B at  $z = 0$ ). For clarity, we shift the results of the three higher mass bins horizontally. The sign of  $b_v - 1$  not only changes with redshift, but also with mass.

$b_v(k) - 1$  can have either negative or positive sign. This challenges the peak mode, which predicts a negative sign. The sign of  $b_v - 1$  does not vary with  $k$ . Furthermore,  $|b_v(k) - 1|$  increases with  $k$ , and roughly speaking  $b_v(k) - 1 \propto k^2$ . (1) At  $k \leq 0.1h/\text{Mpc}$ , the deviation is very weak. Over all the halo mass and redshift investigated, the deviation is 0.3% or less and it is statistically insignificant.  $|b_v - 1|$  is orders of magnitude weaker than the peak model prediction on proto-halos. It means that we can not simply extrapolate the predictions on proto-halo velocity to real halo velocity. (2) At  $0.1 \leq k \leq 0.2h/\text{Mpc}$ ,  $b_v$  may show statistically significant deviation from unity. Depending on the type of halos, the deviation may reach 1%. As discussed later, despite its weakness, it will become a significant source of systematic error for DESI RSD cosmology. (3) At  $0.2 \leq k \leq 0.4h/\text{Mpc}$ , some halo samples show  $\mathcal{O}(10\%)$  deviation from unity. One task of RSD cosmology is to extract cosmological information deep into the nonlinear regime of  $k \leq 0.5h/\text{Mpc}$  (e.g., the cosmic vision dark energy report (Dodelson et al. 2016)). The existence of significant deviation of  $b_v$  from unity at this regime is a challenge to this task.

#### 4.2. The mass and redshift dependence

$b_v$  increases with increasing redshift (Fig. 2, 3 & 4) and decreasing mass (Fig. 5). As a consequence, the sign of  $b_v - 1$  depends on halo mass and redshift. For example,  $b_v - 1$  is always negative for halos of  $M > 10^{13}M_\odot/h$  at all redshifts (Fig. 2). But it changes from positive at  $z = 0$  to negative at  $z = 2$  for less massive halos (Fig. 3 & 4). Another consequence is that  $b_v - 1$  has strong dependence on the halo mass and redshift. For example, for  $M > 10^{13}M_\odot/h$  halos at  $0.25 < k < 0.3h/\text{Mpc}$  and  $z = 1(2)$ ,  $b_v - 1 = -0.026(-0.069)$ . But for halos of  $10^{12} < M < 10^{13}M_\odot/h$ ,  $b_v - 1 \sim 0.3\%$  at  $z = 1$ . Fig. 5 compares  $b_v$  of various mass at  $z = 0$ . Now the biggest

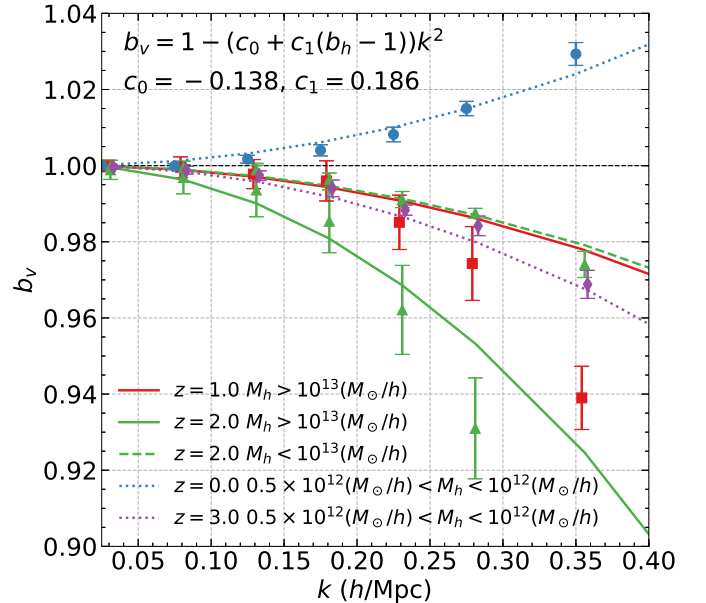


**Figure 6.** A fitting formula of  $b_v$ . For clarity, we do not show the results of all halo sets. The residual error mainly arises from the dependence of the velocity bias  $b_v$  beyond the density bias  $b_h$ . It is an issue for further investigation.

deviation from unity happens for the least massive halos.

To translate the above results into impact on peculiar velocity cosmology, we need specifications of galaxy surveys, since different surveys probe different galaxies in different halos and different redshifts. Here we just present a qualitative description on halos that may be probed by various surveys. Later will quantify the impact of velocity bias to some of these surveys in §5. (1)  $10^{13}M_\odot$  halos at  $z < 1$  may be probed by LRGs in DESI (e.g. Guo et al. (2015); DESI Collaboration et al. (2016)). Galaxies in the TAIPAN redshift and peculiar velocity survey are also expected to reside in these halos, but at  $z \sim 0$  (Howlett et al. 2017). (2) For smaller halos ( $\lesssim 10^{13}M_\odot$ ), 21cm surveys may be capable of detecting them. SKA are capable of detecting billions of 21cm emitting galaxies residing in these halos, given its sensitivity in HI mass (Abdalla & Rawlings 2005; Yang & Zhang 2011) and the observationally constrained HI mass-halo mass relation (e.g. Guo et al. (2017)). SKA is also able to indirectly detect them through the intensity mapping. (3) For halos of  $M < 10^{12}M_\odot$ , a large fraction of ELGs in surveys such as DESI and PFS may reside in these halos (Favole et al. 2016; Gonzalez-Perez et al. 2017). DESI can probe them at  $0.6 \leq z \leq 1.6$  while PFS can probe them to higher redshift ( $z \leq 2.4$ ). 21cm intensity mapping surveys such as CHIME (Bandura et al. 2014) and Tianlai (Xu et al. 2015) are also sensitive to these halos, although they may not be able to detect individual galaxies.

#### 4.3. The dependence on the halo density bias

An interesting observation is that the mass and redshift dependence of  $b_v$  may be absorbed into a single dependence on the halo density bias  $b_h$ . This can be seen by first checking  $b_h$  in the table 1 and then comparing  $b_v$  of halos with similar  $b_h$ . More explicitly, halos of set C (Table 1) at different redshifts are chosen to have

identical density bias ( $\simeq 1$ ). Table. 2 shows that they have roughly the same velocity bias. This motivates us to propose the following fitting formula,

$$b_v(k|M, z) \simeq 1 - [c_0 + c_1(b_h(M, z) - 1)]\tilde{k}^2. \quad (6)$$

Here  $\tilde{k} \equiv k/(\text{Mpc}/h)$ . This is basically the Taylor expansion of  $b_v(\mathbf{k})$  around  $(0, 0, 0)$ . The isotropy of the velocity bias ( $b_v(\mathbf{k}) = b_v(k)$ ) requires that terms of odd power in  $k$  such as  $k_m$  and  $k_mk_nk_l$  ( $m, n, l = 1, 2, 3$ ) vanish in the Taylor expansion. Therefore the leading order term is  $k^2$ . We find that  $c_0 = -0.138 \pm 0.01$  and  $c_1 = 0.186 \pm 0.007$  (Fig. 6). Small error in  $c_1$  shows that the dependence on  $b_h$  is statistically significant. We caution that this fitting formula is only approximate, since it ignores dependence beyond  $b_h$  and ignores higher order  $k$  dependence (e.g.  $k^4$ ). Nevertheless, it is sufficient to describe the over dependence of the velocity bias on halo property and scale (Fig. 6). Another caveat in this fitting formula is the implicit assumption that all the cosmological dependences are encoded in the cosmological dependence of  $b_h$  and therefore  $c_{0,1}$  do not depend on cosmology. This is motivated by the primary dependence of  $b_v$  on  $b_h$ . If valid, we are then able to use this fitting formula for other cosmologies such as the Planck 2015 cosmology (Planck Collaboration et al. 2016), whose  $\Omega_m$  is 13% larger. Future works will use simulations of different cosmologies to investigate this assumption.

## 5. IMPLICATIONS FOR PECULIAR VELOCITY SURVEYS

We discuss two implications of velocity bias on cosmology. The first is that it may bias the structure growth rate measurement in spectroscopic redshift surveys. The second is that it may open a window of testing the equivalence principle at cosmological scales.

### 5.1. Impact on structure growth rate constraint

A major task of cosmological surveys is to constrain the structure growth rate through peculiar velocity. The velocity bias, if ignored or modelled inappropriately, will become a source of systematic error. Whether it is of statistical significance depends on surveys and galaxy types. The low redshift TAIPAN survey aims to measure the peculiar velocities of  $\sim 10^4$  galaxies. It will constrain  $f\sigma_8$  at  $z \sim 0$  with  $\sim 10\%$  accuracy, using information at  $k < 0.2h/\text{Mpc}$  (Howlett et al. 2017). The target galaxies (with  $M \sim 10^{13}M_\odot/h$ ) have  $|b_v - 1| \ll 1\%$  at  $k < 0.2h/\text{Mpc}$  (Fig. 2 and Table 2). Therefore the usual assumption of  $b_v = 1$  results into negligible systematic error, and can be adopted safely.

On the other hand, the spectroscopic redshift survey DESI can measure  $f\sigma_8$  to 1% level over a number of redshift bins, and resulting into an overall 0.4% statistical error (DESI Collaboration et al. 2016). Fig. 7 plots the predicted  $b_v$  of various galaxies in DESI. We estimate  $b_v$  using the fitting formula of Eq. 6. The density biases of various galaxy types are adopted as  $b_{\text{LRG}} = 1.7/D(z)$ ,  $b_{\text{ELG}} = 0.84/D(z)$  and  $b_{\text{QSO}} = 1.2/D(z)$  (DESI Collaboration et al. 2016). Here  $D(z)$  is the linear density growth rate and it is normalized as unity at  $z = 0$ . For DESI, we are no longer able to approximate  $b_v = 1$ , otherwise systematic error at  $1\sigma$  level can be induced.

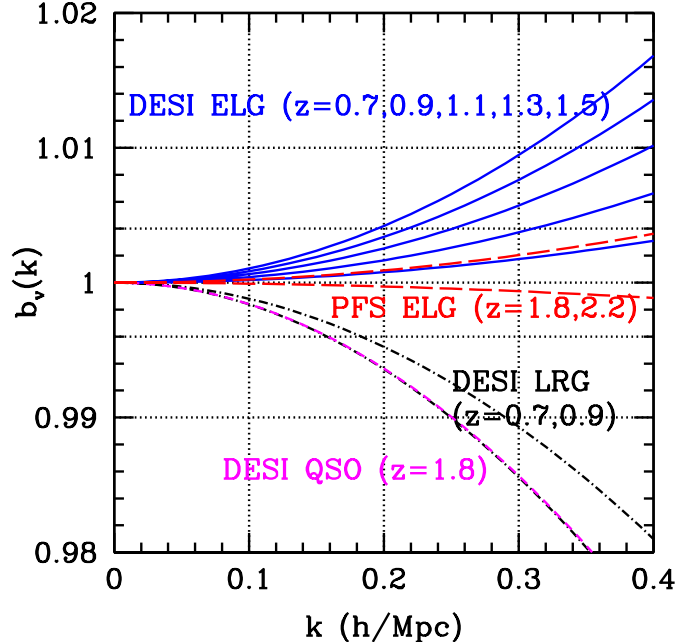


**Figure 7.** Implications for RSD surveys. Notice that the line of DESI LRGs at  $z = 0.9$  almost overlaps with that of DESI QSO at  $z = 1.8$ . (1) The dot lines of  $1 \pm 0.4\%$  denote the expect overall statistical error in  $f\sigma_8$  constrained by DESI. For DESI, velocity bias is a source of significant systematic errors. (2) The velocity bias will be more significant for Euclid, SKA HI survey and the proposed stage V billion object spectra survey, due to their better constraining power in  $f\sigma_8$ . (3) It is less significant for PFS due to its larger statistical error ( $\sim 1\%$ ). Since  $b_v$  of PFS ELGs at  $z < 1.6$  is similar to that of DESI ELGs, we only show the PFS results at  $z = 1.8$  and  $2.2$ .

For PFS ELGs, the predicted  $b_v$  at  $z < 1.6$  is similar to that of DESI ELGs. So for clarity we neglect them in Fig. 7. We only show the results at  $z = 1.8(2.2)$ , where we adopt  $b_{\text{ELG}} = 1.62(1.78)$  (the PFS SSP proposal). If only using information at  $k \leq 0.2h/\text{Mpc}$ , the systematic error in  $f\sigma_8$  caused by ignoring  $b_v \neq 1$  is by less than 0.4%. Due to a factor of 10 smaller sky coverage than DESI, the overall statistical error of  $f\sigma_8$  constrained by PFS RSD to  $k = 0.2h/\text{Mpc}$  is expect to be  $\sim 1\%$ . Therefore the impact of velocity bias on PFS RSD is subdominant and we can simply approximate  $b_v = 1$ . However, due to higher number density of PFS galaxies, it can measure RSD to smaller scales and has the potential to further reduce the statistical error in  $f\sigma_8$ . Fig. 7 shows that, if we push to  $k_{\text{max}} = 0.3h/\text{Mpc}$ , we may no longer adopt  $b_v = 1$ .

The proposed SKA HI survey has the capability of detecting  $\sim 10^9$  21cm emitting galaxies to  $z \lesssim 2$  over  $30000 \text{ deg}^2$  (Abdalla et al. 2015). The statistical error in  $f\sigma_8$  is  $\sim 0.3\%$  for each  $\Delta z \sim 0.1$  redshift bins over  $0.4 < z < 1.3$ . If assuming  $b_v = 1$ , the induced systematic error will overwhelm the statistical error. This will also be true for the proposed stage V survey of measuring a billion spectra of LSST galaxies (Dodelson et al. 2016). The situation for Euclid may fall between DESI and SKA.

### 5.2. A cosmological test of the equivalence principle

Velocity bias also provides a new test of  $\Lambda\text{CDM}$  cosmology. Observationally we are not able to measure

the velocity bias (with respect to dark matter) directly. However, we are able to measure the ratio of velocity bias between two tracers of the large scale structure (LSS). Furthermore, if the two tracers overlap in space, the measured ratio will be free of cosmic variance (McDonald & Seljak 2009). Our result predicts that in  $\Lambda$ CDM, the velocity ratio of two tracers is

$$\frac{b_{v,1}(k)}{b_{v,2}(k)} - 1 \simeq b_{v,1}(k) - b_{v,2}(k) \\ \simeq -0.19\% \left( \frac{k}{0.1h/\text{Mpc}} \right)^2 \times (b_{h,1} - b_{h,2}) \quad (.7)$$

The first approximation holds since  $b_v = 1$  at leading order. This weak deviation from unity is a genuine consequence of the equivalence principle (EP). Therefore if 1% or large deviation at  $k < 0.2h/\text{Mpc}$  is detected, it may be a smoking gun of EP violation and therefore modifications of general relativity (e.g. Hui et al. (2009)). We will further investigate this issue in future works.

## 6. DISCUSSIONS AND CONCLUSIONS

We invent a novel method to determine the volume weighted halo velocity bias  $b_v$ . This method is free of the long-standing sampling artifact problem, which has hindered accurate determination of velocity bias. We apply it to a 3072<sup>3</sup> particle simulation and measure  $b_v$  to  $k \sim 0.4h/\text{Mpc}$  with better than 1% accuracy. Our findings confront both the  $b_v = 1$  standard assumption in peculiar velocity data analysis, and the peak model prediction. (1) There exists statistically significant deviation of  $b_v$  from unity at  $k > 0.1h/\text{Mpc}$ . Depending on halo mass, redshift,  $b_v - 1$  may reach  $\mathcal{O}(1\%)$  at  $k \sim 0.2h/\text{Mpc}$  and  $\mathcal{O}(10\%)$  at  $k \sim 0.4h/\text{Mpc}$ . If ignored, this velocity bias will become a significant source of systematic error in RSD cosmology of DESI. Its impacts on SKA HI

galaxy survey and Euclid are even stronger. (2) However,  $|b_v - 1|$  is a factor of  $\sim 10$  smaller than the prediction of peak model. Furthermore, its mass and redshift dependence do not agree with the peak model prediction.  $b_v$  varies with redshift, while the peak model predicts the opposite.  $b_v$  of less massive halos can be bigger than unity, while the peak model always predicts  $b_v < 1$ . The peak model is based on proto-halo statistics. Therefore we have to consider the mis-match between proto-halos and real halos, and the displacement of halos from the corresponding proto-halos, to improve the theoretical understanding of velocity bias. Another issue to consider is the displacement of halos from their initial positions (Lagrangian positions) to the present positions (Eulerian positions). This affects the velocity correlation, which is defined in Eulerian space. It is expected to make  $b_v$  larger than the peak model prediction, and make it increasing towards  $z = 0$ . We also expect that the environment that halos reside (e.g. filaments or clusters) may play a role in the halo velocity bias. For example, the infall velocity within filaments may be responsible or partly responsible to the  $b_v > 1$  behavior of less massive halos.

There are many issues for further investigations. For example, since the velocity bias depends on the density bias, would it also depend on the halo formation time? Or more general, besides the density bias, what could affect the velocity bias? How does it depend on parameters within the standard cosmology? How does it behave in modified gravity cosmology? Also, to robustly predict its impact on RSD cosmology, we need to generate realistic mocks for target surveys and measure the velocity bias of LRGs, ELGs, 21cm emitting galaxies, etc.

## ACKNOWLEDGMENTS

This work was supported by the National Science Foundation of China (11621303, 11433001, 11653003, 11320101002, 11533006), National Basic Research Program of China (2015CB85701, 2015CB857003).

## APPENDIX

### THE ALGORITHM TO SOLVE FOR THE SCALE DEPENDENT VELOCITY BIAS

Here we describe in details the procedure of solving for the scale dependent  $b_v(k)$ . The key is the statement in §2, that  $b_v(k)$  is the only unknown quantity in Eq. 4, where all other quantities are provided by the same simulation. The proof is as follows. In Fourier space, we can decompose  $\mathbf{v}_h(\mathbf{k}) = b_v(k)\mathbf{v}_m(\mathbf{k}) + \mathbf{v}_h^S(\mathbf{k})$ . The first term is completely correlated with the density velocity field. In contrast, the second term  $\mathbf{v}_h^S$  is the stochastic component of halo velocity. It is uncorrelated to the density velocity field at two-point level. Namely,  $\langle \mathbf{v}^S(\mathbf{k}) \cdot \mathbf{v}_m^*(\mathbf{k}) \rangle = 0$  ( $\langle \mathbf{v}^S(\mathbf{x}_1) \cdot \mathbf{v}_m(\mathbf{x}_2) \rangle = 0$ ). One can verify that the above condition leads to Eq. 5 as the definition of  $b_v(k)$ . The decomposition above is therefore uniquely fixed. Clearly,  $\mathbf{v}_h^S$  does not contribute to  $P_{v_h v_m}$ . Furthermore it does not contribute to  $B_{\delta_h v_h v_m}(k)$ . The direction of  $\hat{v}_h^S(\mathbf{x}_1)$  is uncorrelated with  $\delta_h(\mathbf{x}_1)$  due to the statistical isotropy of the Universe. This holds no matter the halo density bias is scale dependent or non-local, otherwise the statistical isotropy will be violated. The direction of  $\hat{v}_h^S(\mathbf{x}_1)$  is also uncorrelated with  $\mathbf{v}_m(\mathbf{x}_2)$ , by definition. Averaging over its direction, we have  $\langle \delta_h(\mathbf{x}_1) \mathbf{v}_h^S(\mathbf{x}_1) \cdot \mathbf{v}_m(\mathbf{x}_2) \rangle_{\hat{v}_h^S} = 0$ . Therefore  $\mathbf{v}_h^S$  does not contribute to the right hand side of Eq. 4. Since we know  $\delta_h(\mathbf{x})$  and  $\mathbf{v}_m(\mathbf{x})$  from the same simulation,  $b_v(k)$  is all we need to fix the right hand side of Eq. 4.

We are then able to determine  $b_v(k)$  uniquely. The only complexity in determining  $b_v(k)$  is the non-local dependence of the right hand side of Eq. 4 on  $b_v(k)$ . It is caused by  $B_{\delta_h v_h v_m}(k)$ , in which  $b_v(k' \neq k)$  also contributes. Here we present the maximum likelihood solution to  $b_v(k)$ .

We bin the unknown  $b_v(k)$  into a number of  $k$  bins, each with central value  $k_\alpha$  and bin width  $\Delta k_\alpha$  ( $\alpha = 1, 2, \dots$ ).  $b_v(k) = \sum_\alpha b_\alpha W_\alpha(k)$ .  $W_\alpha(k) = 1$  if  $k_\alpha - \Delta k_\alpha/2 < k \leq k_\alpha + \Delta k_\alpha/2$ , and zero otherwise.  $b_\alpha$  is the averaged value of  $b_v$  in the range  $k_\alpha - \Delta k_\alpha/2 < k \leq k_\alpha + \Delta k_\alpha/2$ . The power spectrum  $B_{\delta_h v_h v_m}(\mathbf{k}) = \sum_\alpha b_\alpha B_\alpha(\mathbf{k})$ . Here  $B_\alpha(\mathbf{k})$  is  $B_{\delta_h v_h v_m}(\mathbf{k})$  in which we replace  $\mathbf{v}_h(\mathbf{k}')$  with  $\mathbf{v}_m(\mathbf{k}')W_\alpha(k')$ . The calculation of  $B_\alpha(\mathbf{k})$  is done with several FFTs. First we obtain  $\mathbf{v}_m(\mathbf{k})$  from the simulated  $\mathbf{v}_m(\mathbf{x})$ . We then inverse Fourier transform  $\mathbf{v}_m(\mathbf{k})W_\alpha(k)$  and denote it as

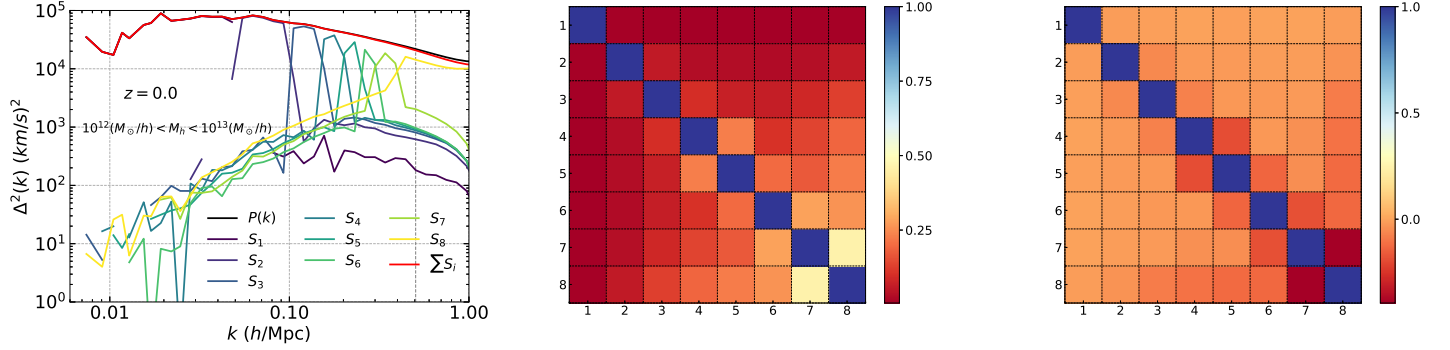


**Figure 8.** The left panel shows  $S_\alpha(k)$  ( $\alpha = 1, 2, \dots$ ) defined in Eq. A1, the sum  $\sum S_\alpha$ , and  $P_{(1+\delta_h)v_h v_m}(k)$  of halos. For brevity, we only show the case of halos in the mass range  $10^{12} < M/(M_\odot/h) < 10^{13}$  and at  $z = 0$ . If the halo velocity bias equals unity,  $\sum S_\alpha = P_{(1+\delta_h)v_h v_m}(k)$ . Slight difference between  $\sum S_\alpha$  and  $P_{(1+\delta_h)v_h v_m}(k)$  (in particular at high  $k$ ) implies that the velocity bias of corresponding halos is close to, but not exactly, unity. We only use the measurement at  $k < 0.5h/\text{Mpc}$  for fitting  $b_v$ . **The middle panel** shows the normalized matrix  $\mathbf{F}_{\alpha\beta}/\sqrt{\mathbf{F}_{\alpha\alpha}\mathbf{F}_{\beta\beta}}$  of Eq. A4. Due to overlap of  $S_\alpha$  and  $S_{\beta\neq\alpha}$  in the  $k$  space,  $F_{\alpha\beta}$  has non-vanishing off-diagonal elements. **The right panel** shows the normalized error matrix  $\mathbf{E}_{\alpha\beta}/\sqrt{\mathbf{E}_{\alpha\alpha}\mathbf{E}_{\beta\beta}}$  in Eq. A5. Overlaps between pairs of  $S_{\alpha\neq\beta}$  in the  $k$  space (the left panel) cause  $F_{\alpha\neq\beta} \neq 0$  (the middle panel), which leads to  $\mathbf{E}_{\alpha\neq\beta} \neq 0$  (the right panel). This results into correlated error in the determined  $b_{1,2,\dots}$ . It is also partly responsible for the increasing statistical error in the determined  $b_v$  with increasing  $k$ .

$\mathbf{v}_\alpha(\mathbf{x})$ . Finally we Fourier transform  $\delta_h(\mathbf{x})\mathbf{v}_\alpha(\mathbf{x})$ , multiply it by  $\mathbf{v}_m^*(\mathbf{k})$ , and obtain  $B_\alpha(\mathbf{k})$ . The estimated/modelled power spectrum is then

$$\hat{P}_{(1+\delta_h)v_h v_m}(\mathbf{k}) = \sum_\alpha b_\alpha (W_\alpha(k)P_{v_m v_m}(\mathbf{k}) + B_\alpha(\mathbf{k})) = \sum_\alpha b_\alpha S_\alpha(\mathbf{k}), \quad S_\alpha(\mathbf{k}) \equiv W_\alpha(k)P_{v_m v_m}(\mathbf{k}) + B_\alpha(\mathbf{k}). \quad (\text{A1})$$

Fig. 8 shows  $S_\alpha$  for halos in the range  $10^{12} < M/(M_\odot/h) < 10^{13}$ . For small  $\alpha$  (small  $k_\alpha$ ),  $S_\alpha$  is dominated by the first term and is very close to a step function in the  $k$  space. But when  $k$  increases, the contribution from  $B_\alpha$  becomes non-negligible. Tails beyond the  $k$  range  $[k_\alpha - \Delta k_\alpha/2, k_\alpha + \Delta k_\alpha/2]$  develop.

Both  $P_{v_m v_m}(\mathbf{k})$  and  $B_\alpha(\mathbf{k})$  are measured from the same simulation, and the only set of unknown parameters are  $b_\alpha$ . Both sides are drawn from the same simulation, therefore the determined  $b_v$  will be essentially free of cosmic variance. The only relevant statistical error in determining  $b_v$  then arises from shot noise in the halo distribution. This allows us to write down the likelihood function  $\mathcal{L} \propto \exp(-\chi^2/2)$  straightforwardly, with

$$\chi^2 = \sum_{\mathbf{k}} \frac{(P_{(1+\delta_h)v_h v_m}(\mathbf{k}) - \hat{P}_{(1+\delta_h)v_h v_m}(\mathbf{k}))^2}{\sigma_{\mathbf{k}}^2}. \quad (\text{A2})$$

$\sigma_{\mathbf{k}}$  is the r.m.s. fluctuation of the data  $P_{(1+\delta_h)v_h v_m}(\mathbf{k})$  caused by the finite number of halos. We estimate it by splitting halos in a given mass bin into 8 non-overlapping sub-samples by randomly selecting among these halos. We measure the dispersion between these sub-samples, divide it by  $\sqrt{8}$  and obtain  $\sigma_{\mathbf{k}}$ . Due to the shot noise origin, the errors are uncorrelated over different  $\mathbf{k}$ .

Since  $\hat{P}_{(1+\delta_h)v_h v_m}$  is a linear combination of  $b_\alpha$  (Eq. A1), the likelihood function  $\mathcal{L}$  of  $b_\alpha$  is a multivariate Gaussian function. The best-fit of  $b_\alpha$  is given by the following linear equations,

$$\frac{\partial \chi^2}{\partial b_\alpha} = 0 \Rightarrow \sum_\beta b_\beta \left[ \sum_{\mathbf{k}} \frac{S_\alpha(\mathbf{k})S_\beta(\mathbf{k})}{\sigma_{\mathbf{k}}^2} \right] = \sum_{\mathbf{k}} \frac{P_{(1+\delta_h)v_h v_m}(\mathbf{k})S_\alpha(\mathbf{k})}{\sigma_{\mathbf{k}}^2}. \quad (\text{A3})$$

The solution (best fit value) is

$$\mathbf{b} = \mathbf{F}^{-1}\mathbf{D}, \quad \text{with } \mathbf{F}_{\alpha\beta} \equiv \sum_{\mathbf{k}} \frac{S_\alpha(\mathbf{k})S_\beta(\mathbf{k})}{\sigma_{\mathbf{k}}^2} \ \& \ \mathbf{D}_\alpha \equiv \sum_{\mathbf{k}} \frac{P_{(1+\delta_h)v_h v_m}(\mathbf{k})S_\alpha(\mathbf{k})}{\sigma_{\mathbf{k}}^2}. \quad (\text{A4})$$

The error covariance matrix  $\mathbf{E}_{\alpha\beta} \equiv \langle \delta b_\alpha \delta b_\beta \rangle$  is given by

$$\mathbf{E}_{\alpha\beta} = (\mathbf{F}^{-1})_{\alpha\beta}. \quad (\text{A5})$$

The matrix  $\mathbf{F}$  and  $\mathbf{E}$  are shown in Fig. 8. Due to overlap of  $S_\alpha$  and  $S_\beta$  ( $\beta \neq \alpha$ ) in the  $k$  space,  $\mathbf{F}$  has non-diagonal elements. They result in correlated error in the determined  $b_\alpha$ , quantified by  $\mathbf{E}_{\alpha\neq\beta} \neq 0$ . The correlation is stronger for pairs of larger  $k_\alpha$  and  $k_\beta$ .

## REFERENCES

Abdalla, F. B., Bull, P., Camera, S., et al. 2015, Advancing Astrophysics with the Square Kilometre Array (AASKA14), 17

- Amendola, L., Appleby, S., Avgoustidis, A., et al. 2016, ArXiv e-prints, arXiv:1606.00180
- Baldauf, T., Desjacques, V., & Seljak, U. 2014, ArXiv e-prints, arXiv:1405.5885
- Bandura, K., Addison, G. E., Amiri, M., et al. 2014, in Proc. SPIE, Vol. 9145, Ground-based and Airborne Telescopes V, 914522
- Bardeen, J. M., Bond, J. R., Kaiser, N., & Szalay, A. S. 1986, ApJ, 304, 15
- Bernardeau, F., & van de Weygaert, R. 1996, MNRAS, 279, 693
- Bernardeau, F., van de Weygaert, R., Hivon, E., & Bouchet, F. R. 1997, MNRAS, 290, 566
- Chan, K. C. 2015, Phys. Rev. D, 92, 123525
- Chan, K. C., Scoccimarro, R., & Sheth, R. K. 2012, Phys. Rev. D, 85, 083509
- Colberg, J. M., White, S. D. M., MacFarland, T. J., et al. 2000, MNRAS, 313, 229
- DESI Collaboration, Aghamousa, A., Aguilar, J., et al. 2016, ArXiv e-prints, arXiv:1611.00036
- Desjacques, V., & Sheth, R. K. 2010, Phys. Rev. D, 81, 023526
- Dodelson, S., Heitmann, K., Hirata, C., et al. 2016, ArXiv e-prints, arXiv:1604.07626
- Elia, A., Ludlow, A. D., & Porciani, C. 2012, MNRAS, 421, 3472
- Favole, G., Comparat, J., Prada, F., et al. 2016, MNRAS, 461, 3421
- Gil-Marín, H., Guy, J., Zarrouk, P., et al. 2018, ArXiv e-prints, arXiv:1801.02689
- Gonzalez-Perez, V., Comparat, J., Norberg, P., et al. 2017, ArXiv e-prints, arXiv:1708.07628
- Guo, H., Li, C., Zheng, Z., et al. 2017, ArXiv e-prints, arXiv:1707.01999
- Guo, H., Zheng, Z., Zehavi, I., et al. 2015, MNRAS, 446, 578
- Hou, J., Sánchez, A. G., Scoccimarro, R., et al. 2018, ArXiv e-prints, arXiv:1801.02656
- Howlett, C., Staveley-Smith, L., & Blake, C. 2017, MNRAS, 464, 2517
- Hui, L., Nicolis, A., & Stubbs, C. W. 2009, Phys. Rev. D, 80, 104002
- Jennings, E., Baugh, C. M., & Hatt, D. 2015, MNRAS, 446, 793
- Jing, Y. P. 2005, ApJ, 620, 559
- Jing, Y. P., Suto, Y., & Mo, H. J. 2007, ApJ, 657, 664
- Kaiser, N. 1987, MNRAS, 227, 1
- McDonald, P., & Seljak, U. 2009, JCAP, 10, 7
- Okumura, T., Seljak, U., & Desjacques, V. 2012, JCAP, 11, 014
- Peebles, P. J. E. 1980, The large-scale structure of the universe, ed. Peebles, P. J. E.
- Planck Collaboration, Ade, P. A. R., Aghanim, N., et al. 2016, A&A, 594, A13
- Pueblas, S., & Scoccimarro, R. 2009, Phys. Rev. D, 80, 043504
- Ruggeri, R., Percival, W. J., Gil Marin, H., et al. 2018, ArXiv e-prints, arXiv:1801.02891
- Schaap, W. E., & van de Weygaert, R. 2000, A&A, 363, L29
- Schlegel, D., Abdalla, F., Abraham, T., et al. 2011, ArXiv e-prints, arXiv:1106.1706
- Scoccimarro, R. 2004, Phys. Rev. D, 70, 083007
- Seljak, U., & McDonald, P. 2011, JCAP, 11, 39
- Spiegel, D., Gehrels, N., Baltay, C., et al. 2015, ArXiv e-prints, arXiv:1503.03757
- Taruya, A., Nishimichi, T., & Saito, S. 2010, Phys. Rev. D, 82, 063522
- White, M., Reid, B., Chuang, C.-H., et al. 2015, MNRAS, 447, 234
- Xu, Y., Wang, X., & Chen, X. 2015, ApJ, 798, 40
- Yang, X., & Zhang, P. 2011, MNRAS, 415, 3485
- Yu, Y., Zhang, J., Jing, Y., & Zhang, P. 2015, Phys. Rev. D, 92, 083527
- . 2017, Phys. Rev. D, 95, 043536
- Zarrouk, P., Burtin, E., Gil-Marín, H., et al. 2018, ArXiv e-prints, arXiv:1801.03062
- Zhang, P., Pan, J., & Zheng, Y. 2013, Phys. Rev. D, 87, 063526
- Zhang, P., Zheng, Y., & Jing, Y. 2015, Phys. Rev. D, 91, 043522
- Zhao, G.-B., Wang, Y., Saito, S., et al. 2018, ArXiv e-prints, arXiv:1801.03043
- Zheng, Y., Zhang, P., & Jing, Y. 2015a, Phys. Rev. D, 91, 123512
- . 2015b, Phys. Rev. D, 91, 043523
- Zheng, Y., Zhang, P., Jing, Y., Lin, W., & Pan, J. 2013, Phys. Rev. D, 88, 103510